Design and Experimental Implementation of Longitudinal Control for Automated Transit Buses

Bongsob Song*
Department of Mechanical Engineering
Ajou University
bsong@ajou.ac.kr

J. Karl Hedrick†
Department of Mechanical Engineering
University of California
khedrick@me.berkeley.edu

***Abstract*— This paper presents the design and experimental implementation of longitudinal control for automated transit buses. Using the rich set of information available via in-vehicle serial data networks and sensors, it is shown how the modeling can be simplified and validated effectively. Furthermore, the control model will be unified to consider both a 40-foot transit bus and a 60-foot articulated bus. A longitudinal controller based on a nonlinear control technique, called dynamic surface control (DSC), is designed for the speed and distance following. This approach allows us to reduce the complexity of the controller as well as time for experimentally tuning the controller gains. Finally, the performance of the proposed longitudinal controller for two different types of transit buses will be shown through experimental tests in the terms of speed and distance tracking errors.**

I. INTRODUCTION

Automation technologies applied to heavy vehicles have recently received significant attention for automated highway systems (AHS) [1], [2]. This attention is due to the potential for earlier deployment compared to passenger cars because of the benefits of increased efficiency and the smaller impact of automation on the overall vehicle cost. Among the class of heavy duty vehicles, transit bus automation can also improve accessibility and quality of service through precision docking, as well as providing additional fuel efficiency and emissions reduction through line-haul automation.

Many control techniques for longitudinal control of both a passenger car and a heavy-duty truck have been developed over the past decade [3], [4], [5]. Furthermore, the feasibility of AHS technology was demonstrated successfully in 1997 by California PATH [6], [7]. However, few studies have been done for automated transit buses, despite the advantages mentioned above. Therefore, the contribution of this paper is to show how existing longitudinal control techniques can be applied and extended to a new system platform, i.e., both a 40-foot transit bus powered by a compressed natural gas (CNG) engine and a 60-foot articulated bus powered by a diesel engine.

The paper will focus on the topics of modeling and longitudinal controller design due to its limited length. However, an overall controller structure including lateral control and driver-vehicle interface (DVI) was developed and implemented on the California PATH transit buses in a demonstration of automated public transportation technology in San Diego, California in August of 2003. The remainder of the paper is divided into six sections. In Section III, schematic of the hardware setup is presented briefly, while the definitions of variables are listed in Section II. An unified high fidelity vehicle model for both a 40-foot transit and 60-foot articulated bus is proposed using a combination of first principles and empirical data in Section IV. Then, the longitudinal controller design for the speed and distance following is discussed within the framework of dynamic surface control (DSC) in Section V. Finally, experimental results will be shown in Section VI, while some conclusions will follow in Section VII.

∗Corresponding author, Yeongtong-gu, Suwon 443-749, Korea, Tel: 1-510-231-5758 Fax: 1-510-231-9512

†Berkeley, CA 94720, USA Tel: 1-510-642-2482 Fax: 1-510-642-6163

II. NOMENCLATURE

v	velocity of the vehicle
a	acceleration of the vehicle
T_e	net engine torque
T_{acc}	accessory engine torque
T_{fric}	nominal frictional engine torque
T_{cmd}	torque control command via J1939
T_b	braking torque
T_{tr}	transmission retarder braking torque
T_{pn}	pneumatic braking torque
F_r	rolling resistance force
F_a	aerodynamic drag force
P_b	brake pressure
h	effective wheel radius
C_a	aerodynamic drag coefficient
C_r	rolling resistance coefficient
J_e	rotational inertia of engine
J_w	rotational inertia of wheels
m	total mass of the vehicle
R_t	gear ratio in transmission
R_f	final drive ratio
R_g	effective gear ratio, i.e., $R_t \times R_f$
Δt_e	pure time delay due to torque control command
τ_g	time constant for gear shifting delay
τ_e	time constant for engine actuator delay
τ_b	time constant for brake actuator delay
Δt_b	pure time delay during braking process
K_b	brake torque coefficient
P_{bv}	brake valve pressure
P_{po}	push-out pressure

u_α accelerator pedal position
u_β brake control command

III. Hardware Setup

The system platforms considered in this paper are a 40-foot transit and a 60-foot articulated bus powered by a CNG engine and a diesel engine, respectively. However, the similar additional hardware setup may be used for the longitudinal control, although the type of engines, and their dimensional sizes and weights are different each other. For example, Fig. 1 shows a schematic of additional hardware setup on the 40-foot transit bus of California PATH. Besides the stock vehicle electronics initially installed by the transit bus manufacturer, such as the engine control module (ECM) and all of the in-vehicle sensors, in addition a PC-104 computer, a vehicle-to-vehicle communication system, a driver-vehicle interface (DVI), a radar and lidar sensor, and a brake actuator have been implemented for longitudinal control on both the 40-foot and 60-foot buses (see in Fig. 1). Among the stock vehicle electronics, the role of ECM is to directly control the operation of the engine based on powertrain information obtained through the in-vehicle serial data networks and the driver pedal inputs. More specifically, the SAE J1939, which is a CAN protocol with 256 Kbits/sec speed or higher [10], is used as the standard in-vehicle network.

Compared with the electronic hardware setup of the automated passenger vehicle of California PATH [6], [7], one of the salient features is that the control computer can communicate with the ECM to access vehicle state information via in-vehicle networks. This has many potential advantages including a reduction in the amount of additional hardware and a potentially simpler control model. For example, lock-up status of the torque converter and gear ratio are available through SAE J1939 [10], which allows the controller to use this information directly rather than estimate the values from a complicated torque converter and transmission model.

IV. Control Model

The purpose of the control model is for the development of a model-based controller. Hence, the model should be complex enough to capture dynamic characteristics of the system, and simple enough to make the controller efficient for real-time application. In this section, it will be shown how the control model can be simplified with information via the J1939 bus. Moreover, the control model will be unified in the sense that the equations of motion between two transit bus models are so similar except minor differences.

A. Longitudinal Equation of Motion

Before deriving the longitudinal dynamics of the bus, the considered assumptions are summarized as follows:

A1) A symmetric rigid body of vehicle chassis
A2) No slip between the wheels and ground, i.e., $v = \omega_w \cdot h$
A3) The torque converter is locked, i.e., $\omega_w = \omega_e \cdot R_g$

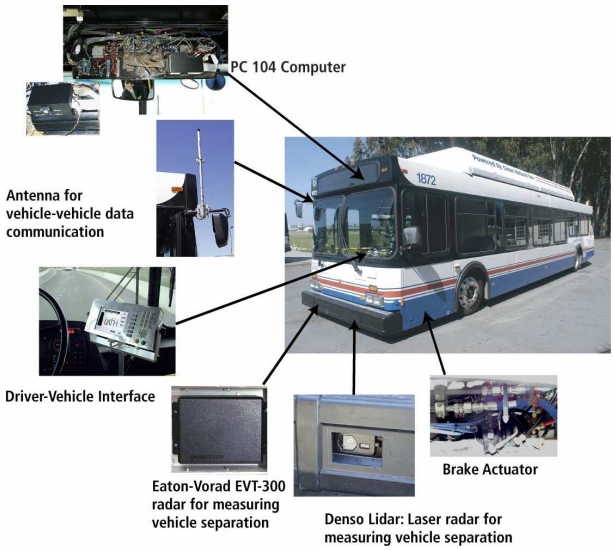

Fig. 1. Schematic of an electronic hardware setup

A4) The accessory engine power is constant, i.e., $T_{acc} \cdot \omega_e = C(\text{A/C, fan}, \ldots)$
A5) The vehicle mass and road grade are known a priori

It is noted that the constant value in A4) relies on the status of an air conditioner (A/C), a fan, and thermal conditions. Moreover, huge change of the mass and road grade has large impact on the longitudinal vehicle dynamics. Therefore, if they cannot be pre-determined, the estimation technique of these values may be necessary, e.g., one of them can be found recently in [11].

Using assumptions A1)- 3) and balancing the forces in the longitudinal direction, we can derive the longitudinal equation of motion. However, these longitudinal dynamics were introduced in [12] and similarly used for the passenger vehicle [8]. For the brevity of the paper, the resulting single state dynamics are derived without detailed descriptions as follows:

$$\dot{v} = \frac{T_e - T_{acc} - R_g T_b}{J_{eq}} - f_1 \tag{1}$$

where J_{eq} and f_1 represent

$$J_{eq} := \frac{J_e + R_g^2 \cdot (J_\omega + m \cdot h^2)}{R_g h},$$
$$f_1 := \frac{R_g h}{J_{eq}}\{F_a + F_r + mg\sin(\theta)\}$$
$$= \frac{R_g h}{J_{eq}}\{C_a v^2 + C_r mg + mg\sin(\theta)\}.$$

It is remarked that there are three variables in (1) which may vary dramatically with respect to time under the assumptions A4) and 5). That is, we need to have the corresponding models for the production of net engine torque (T_e), brake torque (T_b), and effective gear ratio (R_g), which are discussed next.

B. Engine Model

In general, the characteristics of the engine are highly nonlinear and complicated, no matter what it is either a CNG or a diesel engine [13], [14]. There are even several proprietary engine controllers embedded by the engine manufacturer for the purposes of engine protection, noise and emission reduction [10]. However, regardless the type and complexity of engines, the measurement of the engine torque which is transferred to a transmission may be preferable in the sense that the ultimate goal of the engine model is to estimate the generated engine torque for longitudinal control using any available engine actuator. Despite this intuitive idea, many complex engine models have been developed in the literature to estimate the engine torque due to lack of reliability and accuracy of the torque sensor as well as cost consideration [4], [15]. However, it is interesting to remark that the in-vehicle sensor information available via the J-1939 bus has the indicated engine torque and nominal friction engine torque, which are measured or calculated by the engine manufacturer [10]. Therefore, the measured engine torque is regarded as

$$T_{e,meas} = T_{ind} - \alpha \cdot T_{fric} \tag{2}$$

where α is a tunable parameter which will be identified experimentally later in Section VI.

Two engine control actuator methods are used for two different types of engines as follows: one is to use a torque control command (TCC) via the J-1939 bus for the diesel engine and the other is to use an acceleration pedal command via a analog voltage signal for the CNG engine. Although the use of TCC allows us to control the engine torque directly in the sense that the empirical engine map or data are not necessary, the Cummins CNG engine on the 40-foot New Flyer transit bus does not provide the capability of TCC. Hence, the similar approach used for the gasoline engine control was used for the CNG engine due to their similarities shown in [14]. That is, an empirical engine map is used to capture the characteristics of the CNG engine and its controllers quantitatively. Finally, the dynamics of two engines are represented by the first order lag systems as follows [12]:

$$\dot{T}_e = \frac{1}{\tau_e}\{-T_e + T_{map}(\omega_e, u_\alpha)\} \text{ for a CNG engine} \tag{3a}$$

$$\dot{T}_e = \frac{1}{\tau_e}\{-T_e + T_{cmd}(t - \Delta t_e)\} \text{ for a diesel engine} \tag{3b}$$

where T_{map} is the empirical engine torque map which indicates the net engine torque for the given engine speed and accelerator pedal position, and T_{cmd} is the torque control command via a J1939 bus.

C. Transmission Model

The transmission is also a highly nonlinear and complex system like the engine above. It is generally very hard to derive a simple set of mathematical equations to represent a complete transmission model. However, if (1) is simple enough to capture the equation of motion for the transit bus, only two values are required from the transmission model, i.e., effective gear ratio (R_g) and transmission retarder braking torque (T_{tr}). The former comes from the engaged gear ratio (R_t) multiplied by the final gear ratio. The transmission information directly available from the J1939 bus includes selected and current gear, actual gear ratio, and an index of "shift in progress". However, accurate gear ratio information is not available while a gear shift is occurring. The gear ratio during gear shifting can be estimated as follows: If the shift-in-progress is on,

$$\dot{R}_t = \frac{1}{\tau_g}\{-R_t + R_{sel}\} \tag{4a}$$

Otherwise,

$$R_t = R_{cur} \tag{4b}$$

where R_{sel} and R_{cur} are the selected and current gear ratio, respectively.

The transmission retarder braking torque required from the transmission model is controlled and reported by the J-bus. Although the capacity of the transmission retarder braking torque is limited, its time response is usually faster than one of a pneumatic braking system. Hence, integrated braking approach combining the transmission retarder and pneumatic braking torque is used for the braking control. Then, the overall braking torque can be decoupled as follows:

$$T_b = T_{tr} + T_{pn} \tag{5}$$

Next, it will be discussed in the following section how T_{pn} is produced in the pneumatic brake system.

D. Pneumatic brake model

A schematic of a pneumatic brake system for a front wheel of the transit bus is shown in Fig. 2. While the pressure coming from the dual brake valve in the figure is typically controlled by a driver's foot for manual driving, an electrical brake actuator is implemented in parallel to generate additional brake pressure (P_{bv}). Sequentially, the brake pressure is the maximum of two pressure values through the mixing valve shown in Fig. 2. Assuming that brake torque has a proportional relation with the brake pressure in the diaphragm chamber of a pneumatic brake system and that there is no driver command, the brake pressure dynamics to the brake chamber shown in Fig. 2 can be derived as follows [16]:

$$T_{pn} = \begin{cases} K_b(P_b - P_o) & \text{if } P_b \geq P_o \\ 0 & \text{otherwise} \end{cases} \tag{6a}$$

$$\dot{P}_b = \begin{cases} \frac{1}{\tau_{bf}}[-P_b + P_{bv}\{u_\beta(t - \Delta t_b)\}] & \text{for filling} \\ \frac{1}{\tau_{be}}\{-P_b + P_{bv}(u_\beta)\} & \text{for emptying} \end{cases} \tag{6b}$$

where P_{bv} is an empirical function of the brake control command u_β.

The time responses for step inputs to the pneumatic brake system with an electrical brake actuator are presented

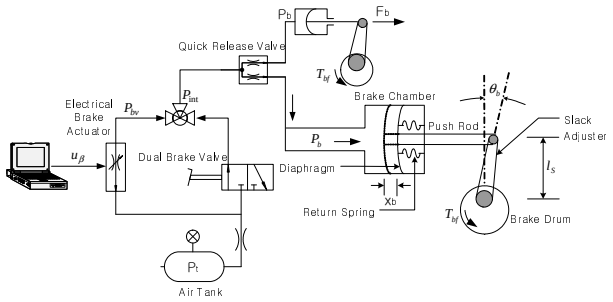

Fig. 2. Schematic of a pneumatic brake system with an electrical brake actuator

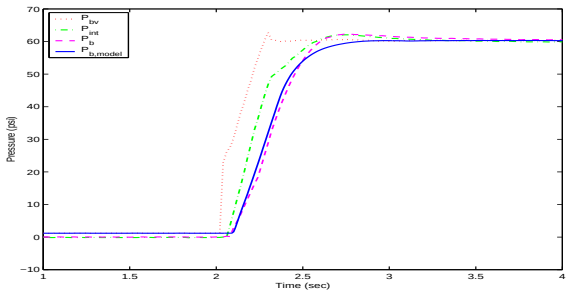

Fig. 3. Time responses of brake pressure

in Fig. 3 when the transit bus is stationary. Three brake pressure measurements from brake pressure transducers located in different positions are shown in the figure: P_{bv} is measured from an embedded sensor in the electrical brake actuator, P_{int} and P_b are measured near the mixing valve and the front wheel, respectively (also see in Fig. 2). Finally, the time response of the brake pressure model shown in (6b) is plotted together to show the accuracy of the proposed model.

V. Longitudinal Controller Design

The objective of the longitudinal controller is to follow either a given desired velocity or distance profile using the three control inputs, namely the engine torque, transmission retarder braking torque, and pneumatic braking torque. Based on the vehicle model proposed in the previous section, the longitudinal controller is designed to achieve desired control objectives.

A. Speed Control via DSC

In this section, the control laws for determining the desired engine and brake torque will be designed using DSC. Due to the successful implementation of DSC previously on the California PATH passenger vehicle [6], [7], and its extensibility to the transit bus models, the speed control law will be derived briefly without detailed descriptions. Using the terminology of sliding mode control, the sliding error surface representing the velocity tracking error is defined as $S_{1e} := v - v_{des}$. Then, after differentiating S_{1e} and using (1), we can write the forcing term $\bar{T}_e$ and filter dynamics as follows:

$$\dot{S}_{1e} = \frac{T_e - T_{acc} - R_g T_b}{J_{eq}} - f_1 - \dot{v}_{des}$$

$$\Longrightarrow \bar{T}_e = T_{acc} + R_g T_b + J_{eq}(f_1 + \dot{v}_{des} - \lambda_{1e} S_{1e}) \quad (7a)$$

$$\Longrightarrow \tau_{2e}\dot{T}_{edes} + T_{edes} = \bar{T}_e, \quad T_{edes}(0) := \bar{T}_e(0) \quad (7b)$$

where T_b is zero for engine control and λ_{1e} is the control gain of the first sliding surface. Subsequently, after differentiating $S_{2e} := T_e - T_{edes}$ and using (3a) and (3b), the subsequent surface error dynamics and desired engine torque command are:

$$\dot{S}_{2e} = \dot{T}_e - \dot{T}_{edes} = \frac{1}{\tau_e}(-T_e + T_{ctrl}) - \dot{T}_{edes}$$

$$\Longrightarrow T_{ctrl} = T_e + \tau_e(\dot{T}_{edes} - \lambda_{2e}\tilde{S}_{2e}) \quad (7c)$$

$$\Longrightarrow \begin{cases} T_{cmd} = T_{ctrl} & \text{for a diesel engine} \\ u_\alpha = q_e(\omega_e, T_{ctrl}) & \text{for a CNG engine} \end{cases} \quad (7d)$$

where $\tilde{S}_{2e} := T_{e,meas} - T_{edes}$, λ_{2e} is the control gain of the second sliding surface, and q_e is an inverse map of $T_{map}(\omega, u_\alpha)$ in (3a). It is noted that the desired engine torque command (T_{ctrl}) is used as TCC for the diesel engine and is fed into the inverse engine map to calculate the pedal position command for the CNG engine. Furthermore, the engine torque value defined in (2) is used to calculate $\tilde{S}_{2e}$, which might be slightly different from S_{2e}.

A control law for the brake system can be derived similarly by defining $S_{1b} := S_{1e}$. After following the similar procedure, the corresponding equations for the brake system are:

$$\bar{T}_b = \frac{1}{R_g}\left[T_{ect} - T_{acc} - J_{eq}(f_1 + \dot{v}_{des} - \lambda_{1b} S_{1b})\right] \quad (8a)$$

$$\tau_{2b}\dot{P}_{bdes} + P_{bdes} = \bar{T}_b / K_b, \quad P_{bdes}(0) := \bar{P}_b(0) \quad (8b)$$

$$\bar{P}_{bv}(u_\beta) = P_b + \tau_b(\dot{P}_{bdes} - \lambda_{2b} S_{2b}) \quad (8c)$$

$$u_\beta = q_b(\bar{P}_{bv}) \quad (8d)$$

where T_{ect} is the minimum or closed throttle torque, $S_{2b} := P_b - P_{bdes}$, and q_b is the inverse function of P_{bv}. Finally, the appropriate choice of the controller gains, $\{\lambda_{1i}, \lambda_{2i}, \tau_{2i}\}$ for $i = e, b$, can be referred to [12] for more detailed discussion.

B. Distance Following Control

The distance following control law can be derived similarly by extending the definition of S_1. Suppose there are only two vehicles, i.e., the leading and following vehicle. The first sliding surface can be defined as

$$S_1 = \dot{\epsilon}_1 + q_1 \epsilon_1 \quad (9)$$

where $\epsilon_1 = R_{des} - R_1$, R_{des} is the desired spacing, and R_1 is the distance between the lead and following vehicle. As derived in (7), both engine and brake control laws can be obtained similarly. Furthermore, it is interesting to remark that both R_1 and $\dot{R}_1$ are obtained through the range and range rate measurement sensors. As shown in Fig. 1, a radar,

a lidar, and a communication system are used to measure the range and range rate. The detailed discussion for the sensor processing and fusion algorithm can be found in [17]. Although this sensor processing and fusion is critical for longitudinal control, it is not discussed due to the limited space of the paper.

If there are more than two vehicles to consider, the first sliding surface can be extended for guaranteeing the string stability [6] as follows: for $i \geq 2$,

$$S_1 = \dot{\epsilon}_i + q_1\epsilon_i + q_2(\dot{x}_{i+1} - \dot{x}_{lead}) + q_3\left(x_{i+1} - x_{lead} - \sum_{j=1}^{i} L_j\right)$$

where $\epsilon_i = R_{des} - R_i$, R_i is the range of $(i+1)$th vehicle, x_i is the position of ith vehicle, and x_{lead} is the position of the first vehicle, and L_j is the length of jth vehicle.

C. Switching Criterion

The specific control mode of the vehicle is determined by switching logic based on the desired and residual acceleration computed by the engine control law. The residual acceleration is defined as

$$a_{resid} = \frac{T_{ect} - T_{acc}}{J_{eq}} - f_1 \qquad (10)$$

and represents the acceleration of the vehicle as a result of closed-throttle-torque, rolling resistance, and aerodynamic drag. For example, if the engine controller computes $a_{syn} \geq a_{resid}$ where $a_{syn} := \dot{v}_{des} - \lambda_{1e}S_{1e}$, then engine control is used. However, if $a_{syn} < a_{resid}$, then brake control is used [8], [6]. Once the brake control is activated, it should be decided whether the transmission retarder braking torque is enough or additionally a pneumatic braking torque is necessary. One of the simplest method is to use the maximum torque of the transmission retarder (T_{max}) as follows:

$$\begin{cases} T_{tr} = \bar{T}_b \\ u_\beta = 0 \end{cases} \quad \text{if } \bar{T}_b \leq T_{max}$$

$$\begin{cases} T_{tr} = T_{max} \\ u_\beta = q_b(\bar{P}_{bv} - T_{max}/K_b) \end{cases} \quad \text{otherwise}$$

It is remarked that small hysteresis for the switching criterion was used to prevent the potential chatter due to sensor noise, finite sampling rate, and model uncertainties [8].

VI. Experimental Results

Experiments were conducted to validate the proposed control model and to verify the longitudinal controller. Again, the system platforms considered in this study are a New Flyer 40-foot transit bus powered by a Cummins compressed natural gas (CNG) engine and a New Flyer 60-foot articulated bus by a Detroit Diesel diesel engine.

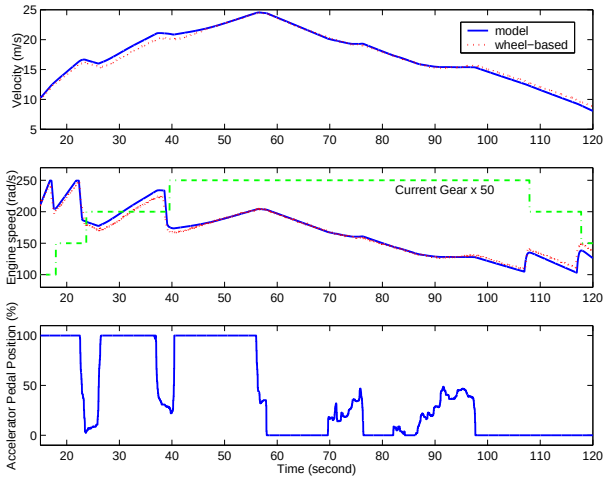

Fig. 4. Time responses of a transit bus driven manually

A. Model Validation

Data acquisition of two types of the transit buses manually driven was performed at the Crow's Landing Test Facility. All information such as wheel-based speed, engine speed, current gear, and an accelerator pedal position were acquired via the J1939 bus. Then, their time responses are compared with the those of the transit bus model proposed in Section IV. For instance, Fig. 4. shows the time responses of the 40-foot transit bus in the operating velocity range from 10 to 25 m/s, during which the gear shifts from 2nd to 5th gear and the torque converter remains locked. With the appropriate system parameters [12], the accuracy of the model shown in Fig. 4 is that the deviation in terms of velocity and engine speed is within 5%. The performance of the 60-foot bus model is quite similar with the one shown in Fig. 4, so the comparison is not shown in the paper for the brevity. However, these results show that the fairly simple and unified model represents longitudinal dynamics of the two transit bus. Next task is to verify whether the longitudinal controller based on the validated model can achieve the control objectives in the terms of speed and distance following.

B. Controller Performance

While the model validation was performed in the flat open space mentioned above, high speed tests using two transit buses were conducted on I-15 in San Diego, California in cooperation with experimental demonstration team members in the California PATH program. The 40-foot CNG bus was driven automatically as a leading vehicle, and the automated 60-foot articulated bus followed with a given desired spacing. Fig. 5(a) shows speed responses of the two transit buses as well as a given desired speed profile with respect to time. The operation of both vehicles was switched to automatic control initially about the speed of 13 m/s by a driver through DVI, and the following distance was closing and opening from 40 m and 20 m after about

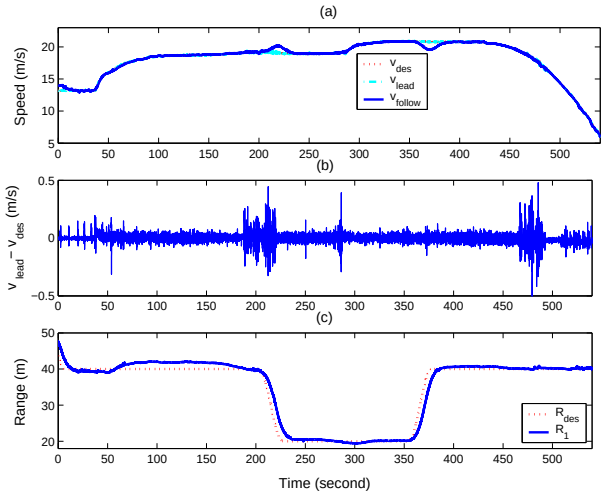

Fig. 5. Experimental velocity and distance following performance

210 and 360 second, respectively. Fig. 5(b) shows that the velocity tracking error of the lead vehicle stays less than 0.5 m/s, which is on the order of the wheel speed sensor resolution [10], while the distance tracking error of the following vehicle is within $2m$ as shown in Fig. 5(c). It is noted that there is a fairly steep hill during the period from 60 to 190 second, and it results in larger distance tracking error. Except this period, the distance tracking error remains in 0.5 m during the constant distance following. It is suggested that it may be good to have a road grade estimation algorithm and the corresponding hardware to improve the distance following performance in the presence of a steep hill on a highway.

VII. Conclusions

This paper developed the longitudinal control for an automated transit bus within the framework of dynamic surface control (DSC). The control model to deal with two types of transit buses was derived and simplified with the advantages of the J1939 in-vehicle serial data network, and unified for the longitudinal controller design. Then, DSC was applied to develop the speed and distance following control laws, and the switching criterion. Finally, the longitudinal controller was validated through high speed closed-loop tests on I-15 in San Diego, California.

VIII. Acknowledgments

The authors would like to thank California PATH demonstration-team members for their contribution regarding a hardware and software setup for the data acquisition and high speed tests. The author has been supported in part by Ajou university research fund for a new faculty member.

References

[1] C. Chen and M. Tomizuka, Steering and independent braking control for tractor-semitrailer vehicles in automated highway systems. *Proceedings of the 34th Conference on Decision and Control*, 1995, pp 1561-1566.

[2] M. Druzhinina, A. Stefanopoulou, and L. Moklegaard, Adaptive continuously variable compression braking control for heavy-duty vehicles. *Journal of Dynamic Systems, Measurement, and Control*, vol. 124, 2002, pp 406-414.

[3] J.K. Hedrick, D. McMahon, V. Narendran, and D. Swaroop, Longitudinal vehicle controller design for IVHS systems, *Proceedings of American Control Conference*, 1991, pp 3107-3112.

[4] S. Choi and J.K. Hedrick, Vehicle longitudinal control using an adaptive observer for automated highway systems, *Proceedings of American Control Conference*, vol.5, 1995, pp 3106-3110.

[5] D. Yanakiev and I. Kanellakopoulos, Longitudinal control of automated CHVs with significant actuator delays. *IEEE Transactions on Vehicular Technology*, vol. 50, no. 5, 2001, pp 1289-1297.

[6] J.K. Hedrick and P.P. Yip, Multiple sliding surface control: theory and application, *Journal of Dynamic System, Measurement, and Control*, vol. 122, December, 2000, pp 586-593.

[7] R. Rajamani, H. Tan, B.K. Law, and W. Zhang, Demonstration of integrated longitudinal and lateral control for the operation of automated vehicles in platoons. *IEEE Trans. Control Systems Technology*, vol. 8, no. 4, 2000, pp 695-708.

[8] J.C. Gerdes, Decoupled design of robust controllers for nonlinear systems: as motivated by and applied to coordinated throttle and brake control for automated highways, *Ph. D. thesis*, U.C. Berkeley, 1996.

[9] D. Swaroop, J.K. Hedrick, Y.Y. Yip, and J.C. Gerdes, Dynamic surface control for a class of nonlinear systems, *IEEE Transactions on Automatic Control*, vol. 45, no. 10, 2000, pp 1893-1899.

[10] *SAE truck and bus control and communications network standards manual*(2001 edn). SAE International, 2001.

[11] H. Bae, J. Ryu, and C. Gerdes, Road grade and vehicle parameter estimation for longitudinal control using GPS, *Proceedings of IEEE Intelligent Transportation Systems Conference*, 2001, pp 166-171.

[12] B. Song, J.K. Hedrick, and A. Howell, Fault tolerant control and classification for longitudinal vehicle control, *Journal of Dynamic Systems, Measurement, and Control*, vol. 125, September, 2003, pp 320-329.

[13] A. Gangopadhyay and P. Meckl, Modeling, validation and system identification of a natural gas engine, *Proceedings of the American Control Conference*, June, 1997, pp 294-298.

[14] R. Weeks and J.J. Moskwa, Transient air flow rate estimation in a natural gas engine using a nonlinear observer, *SAE Transactions*, no. 940759, 1994, pp 1-18.

[15] D. Cho and J.K. Hedrick, Automotive power modeling for control, *Journal of Dynamic Systems, Measurement, and Control*, vol. 111, December, 1989, pp 568-576.

[16] R. Limpert, *Brake design and safety.* SAE, Inc., Warrendale, PA, 1992.

[17] A. Howell, B. Song, and J.K. Hedrick, Cooperative range estimation and sensor diagnostics for vehicle control, *Proceedings of ASME: Dynamic Systems and Control Division*, To appear in Nov. 2003.